Leptogenic supersymmetry

Article (Published Version)

Leptogenic supersymmetry

Andrea De Simone,[1] JiJi Fan,[2] Veronica Sanz,[3,*] and Witold Skiba[2]
[1]*Center for Theoretical Physics, Massachusetts Institute of Technology, Cambridge, Massachusetts 02139, USA*
[2]*Department of Physics, Sloane Laboratory, Yale University, New Haven, Connecticut 06520, USA*
[3]*Physics Department, Boston University, 590 Commonwealth Ave, Boston, Massachusetts 02215, USA*
(Received 24 April 2009; published 12 August 2009)

Leptogenic supersymmetry is a scenario characterized by cascade decays with copious lepton production. Leptogenic models have striking signatures that can be probed by the LHC even in the 10 TeV run with as little as 200 pb^{-1} of data, provided the squark masses are about 1 TeV. Leptogenic supersymmetry spectrum arises in several well-motivated models and its signatures are long-lived sleptons, numerous isolated leptons, abundant Higgs production, rather energetic jets, and no missing energy. The Higgs can be discovered in the $h \to b\bar{b}$ mode via the 4 leptons + 4 jets channel because the leptons accompanying Higgs production suppress the background. The superparticle masses in leptogenic supersymmetry can be measured efficiently due to lack of missing energy and high lepton multiplicity. We estimate that 1 fb^{-1} of integrated luminosity is sufficient to determine the light Higgs, neutralinos, charginos, slepton, sneutrino, and squark masses in a 14 TeV run.

DOI: 10.1103/PhysRevD.80.035010 PACS numbers: 11.30.Pb, 12.60.Jv

I. INTRODUCTION

What makes a leptogenic supersymmetry (lepto-SUSY) is best explained pictorially in Fig. 1. In the spectrum of lepto-SUSY, all the sleptons lie at the bottom. Thus the decay kinematics ensures that multiple leptons are produced in every decay chain. The production of new particles is dominated by QCD production of squarks and gluinos, which are assumed to be at the top of the mass spectrum. Colored particles decay into lighter charginos and neutralinos. The charginos and neutralinos are heavier than the sleptons and therefore decay into leptons and sleptons. All sleptons decay into the lightest slepton which is the next-to lightest supersymmetric particle (NLSP). The NLSP is collider stable and eventually decays into the gravitino. Because the gravitino LSP is created outside detectors it is not shown in Fig. 1.

This particular hierarchy of masses is responsible for collider signals with very little standard model (SM) backgrounds. For example, the leading production mechanisms, $\tilde{q}\,\tilde{q}$ and $\tilde{q}\,\tilde{\bar{q}}$, lead to at least two hard jets from the decays of the two squarks. The two jets are accompanied by two sleptons and a handful of leptons as every supersymmetric particle must decay into the slepton NLSP. Because of the large mass differences between the squarks and sleptons the NLSP sleptons are quite energetic and a large fraction of them have velocities larger than 0.95. Some of the fast sleptons would likely be misidentified as muons and we refer to the misidentified sleptons as leptons. The total number of observed leptons in an event varies depending on the details of the decay chain and how many of the leptons are neutrinos and taus, which are difficult to reconstruct. One expects anywhere between two and eight observed leptons, some of which would be misidentified sleptons, as well as up to two properly identified sleptons. We analyze in detail events with 4, 5, and 6 leptonlike particles, as events with fewer identified leptons have non-negligible backgrounds and events with more leptons are rare.

The decay chains that pass through the heavier sleptons lead to significant Higgs boson production. This happens most of the time for the heavy stau decays and a fraction of the smuon decays as long as the mass splitting between the sleptons is larger than the Higgs mass. The Higgs is then associated with a clean four-lepton signature and can be discovered in the $b\bar{b}$ channel. This is thrilling as for most other scenarios with a light Higgs, the $b\bar{b}$ would not be the first channel to be observed, and in fact that channel may never be observed.

Assuming squark masses of about 1 TeV, we show that very significant excesses in every (4, 5, and 6) lepton channel can be obtained with only 200 pb^{-1} of integrated luminosity in the 10 TeV run of the LHC. Some of the masses can be reconstructed with this little luminosity, while most masses can be determined using 1 fb^{-1} of data collected at 14 TeV.

Our approach is model independent as we parametrize the spectrum and do not make assumptions about its origin. However, lepto-SUSY spectrum does arise in several models. Low-scale gaugino mediation (L$\tilde{g}$M) [1] is a class of models with a parametric suppression of sfermion masses compared to the gauginos. Other examples include gauge mediation (GMSB) [2] with a large number of messengers as well as models with Dirac gaugino masses [3].

The structure of this article is as follows. In the next section, we present a sample spectrum and describe the most important slepton decay channels. In Sec. III, we turn to LHC phenomenology. We discuss events with multiple

*On leave of absence from York University, Ontario, Canada.

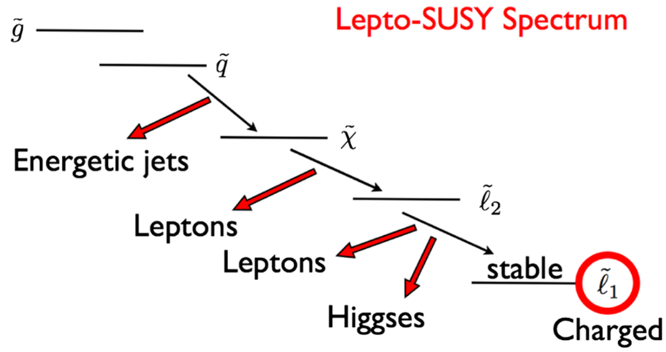

FIG. 1 (color online). Lepto-SUSY spectrum and typical decay channels.

leptons, analyze the most promising Higgs discovery channel, and study spectrum reconstruction. Section IV contains our parametrization of the soft mass terms. We also outline how the lepto-SUSY spectrum is featured in several mediation models. We conclude and outline future directions in Sec. V.

II. LEPTO-SUSY SPECTRUM AND DECAYS

The spectrum of lepto-SUSY is as depicted in Fig. 1, namely,

$$m_{\tilde{g}}, m_{\tilde{q}} > m_{\tilde{\chi}^0}, m_{\tilde{\chi}^\pm} > m_{\tilde{\ell}_L} > m_h, m_{\tilde{\ell}_R}.$$

The gluino can be either lighter or heavier than the squarks. Such ordering of masses emerges in several scenarios of supersymmetry breaking. In Sec. IV, we propose a natural parametrization of the soft mass terms that is applicable to gauge mediated models. In our parametrization, the scalar soft masses are described by four dimensionless numbers and are proportional to the gaugino masses. The gaugino masses are assumed to obey the unified relations so, together with $\tan\beta$ and $\mathrm{sign}\mu$, we have 7 parameters. The details are not crucial for the phenomenological studies we are about to describe and are therefore postponed to Sec. IV.

We impose constraints on the spectrum that ensure correct electroweak symmetry breaking (EWSB), and that the slepton [4] and Higgs masses are above the direct search limits. The Higgs mass is most sensitive to the magnitude of the stop loop correction. The bound $m_h > 114$ GeV implies a lower bound on $m_{\tilde{q}}$, which in the large $\tan\beta$ limit translates to $m_{\tilde{q}} > 700$ GeV.[1] The lightest neutralino $\tilde{\chi}_1^0$ can be either Higgsino-like or bino-like depending on the relative sizes of μ and m_1, where m_i are the gaugino soft mass terms with $i = 1, 2, 3$ corresponding to the SM gauge groups. If $\mu \gg m_1$, $\tilde{\chi}_1^0$ is mostly bino-like while it is Higgsino-like for $\mu \ll m_1$.

[1]This bound is obtained as we neglect the trilinear A-terms. Thus all squarks, including the two stops, are nearly degenerate in mass.

Using these results, we find the bounds on the mass ratios that are relevant to the production and decay channels we will consider:

$$\begin{aligned} &3 > m_{\tilde{q}}/m_2 > 1.1, \qquad 5.8 > m_{\tilde{q}}/m_1 > 2.2, \\ &12 > m_1/m_{\tilde{\ell}_R} > 1, \qquad 26 > m_2/m_{\tilde{\ell}_L} > 1.9, \\ &\mu/m_1 > 0.2. \end{aligned} \tag{1}$$

When the constraints are taken into account, the gap between sleptons and gauginos can be rather large. The supersymmetric standard model (MSSM) spectra are calculated using the SUSY-HIT program [5] and a sample spectrum is shown in Table I. The soft masses and our parameters that yield the sample spectrum are described in Sec. IV.

In our study the trilinear A-terms are set to zero, so the three generations of squarks are nearly degenerate and there is little mixing between the left- and right-handed squarks. Thus all three generation squarks can be produced at a hadron collider. As a consequence, the Higgsinos with significant couplings to the third-generation squarks only could also be produced in cascade decays. Nonzero A-terms contribute the term $Av\sin\beta$ to the off diagonal entries in the squark mass matrix, where $v = 174$ GeV is the EWSB vacuum expectation value. Assuming only the stop A-term, A_t, is large, a sizable mass splitting between the up squarks and stops of order $\delta m \sim 100$ GeV would require $A_t v/(2m_{\tilde{q}}) \sim 100$ GeV in the large $\tan\beta$ limit. For our sample point, $m_{\tilde{q}} \sim 1$ TeV which corresponds to $A_t \sim 1$ TeV. This is unnaturally large in models that lead to the lepto-SUSY spectrum, hence we neglect the effects of the A-terms.

In the sample spectrum in Table I, the NLSP is $\tilde{\tau}_1$. The decay length of the NLSP, produced with energy E, in the laboratory frame is (see, e.g., [2,6])

TABLE I. A sample spectrum calculated with SUSY-HIT using input soft terms described in Sec. IV: $\mu = 294$ GeV, $A = 0$, and $\tan\beta = 10$. All masses are in GeV.

$m_{\tilde{g}}$	1938	$m_{\tilde{u}_L}$	949
$m_{\tilde{\chi}_1^\pm}$	291	$m_{\tilde{u}_R}$	920
$m_{\tilde{\chi}_2^\pm}$	676	$m_{\tilde{d}_L}$	952
$m_{\tilde{\chi}_4^0}$	676	$m_{\tilde{d}_R}$	919
$m_{\tilde{\chi}_3^0}$	353	$m_{\tilde{t}_1}$	920
$m_{\tilde{\chi}_2^0}$	302	$m_{\tilde{t}_2}$	962
$m_{\tilde{\chi}_1^0}$	271	$m_{\tilde{\ell}_L}$	248
m_h	115	$m_{\tilde{\ell}_R}$	108
$m_{H^\pm}$	387	$m_{\tilde{\nu}}$	236
m_A	379	$m_{\tilde{\tau}_1}$	106
m_{H_0}	379	$m_{\tilde{\tau}_2}$	249

$$L(\tilde{\tau}_1 \to \tau \tilde{G}) \simeq 1.7 \sqrt{\frac{E^2}{m_{\tilde{\tau}_1}^2} - 1} \left(\frac{100 \text{ GeV}}{m_{\tilde{\tau}_1}}\right)^5 \left(\frac{m_{3/2}}{10 \text{ keV}}\right)^2 \text{ km}, \tag{2}$$

where $m_{3/2}$ is the gravitino mass. For the typical masses of our model, gravitinos lighter than 1 GeV are cosmologically safe, i.e., they evade the constraints from overclosure of the Universe and big bang nucleosynthesis, provided that the reheating temperature is lower than about 10^7 GeV.

For simplicity, we will assume that $m_{3/2} \sim 10$ keV. Then $\tilde{\tau}_1$ has a very long lifetime and exits detectors without decaying. The other right-handed sleptons, $\tilde{e}_R$ and $\tilde{\mu}_R$, will decay to $\tilde{\tau}_1$ through $\tilde{\ell}_R \to \ell_R \tau_R \tilde{\tau}_R$. Because of the small mass difference $m_{\tilde{e}_R} - m_{\tilde{\tau}_1} - m_\tau = 0.6$ GeV, the lepton and τ produced in the decays have insufficient energy to pass p_T cuts. Larger mass splittings were considered in Ref. [7]. In our case, the decay lengths of $\tilde{e}_R$ and $\tilde{\mu}_R$ are too short to observe an independent track. Even if the decay lengths were long enough to observe tracks, the small mass difference means there will not be visible kinks. Therefore, the phenomenology will resemble that of the ''slepton co-NLSP scenario'' of the well-studied GMSB point G2b [8–10]. Note, though, that the ordering of the light neutralinos/charginos and of the heavier sleptons masses is opposite in lepto-SUSY to that of the G2b point. We now turn to the decays relevant for collider phenomenology.

In lepto-SUSY scenario, Higgsinos and gauginos must decay to the lightest collider-stable SUSY particles, $\tilde{\ell}_1 = \tilde{e}_R$, $\tilde{\mu}_1$, $\tilde{\tau}_1$, and hence produce leptons. The number of leptons depends on whether the neutralinos go through a short ($\tilde{\chi} \to \tilde{\ell}_1$) or through a long ($\tilde{\chi} \to \tilde{\ell}_2 \to \tilde{\ell}_1$) decay chain. Additional leptons and Higgses are produced in the long decay chains. Phase space permitted, $\tilde{\tau}_2$ undergoes a two-body decay into Z or h. Those channels are closed for $\tilde{e}_L$ so the three-body $\tilde{e}_L \to \ell \ell' \tilde{\ell}'_1$ decay dominates. For $\tilde{\mu}_2$, both the two- and three-body decays are open.

A. Leptons galore

In lepto-SUSY, the heavier sleptons can only decay into two leptons and the collider-stable slepton. Same-sign leptons (SSL) are therefore produced at a higher rate than opposite-sign leptons (OSL), which is another remarkable feature of the lepto-SUSY phenomenology.

In the following, we will present analytical results for the three-body decay widths of $\tilde{e}_L$ and $\tilde{\mu}_L$. The effect of mixing will be discussed in Sec. as it is important for the staus and smuons. Here we use the notation of Refs. [7,11].

The number of SSL and OSL is given by

$$\Gamma_{\text{SSL,OSL}} = \Gamma(\tilde{\ell}_L^- \to \ell_L^- \ell_R^\mp \tilde{\ell}_R^\pm) \approx \frac{m_{\tilde{\ell}_L}}{512\pi^3} \sum_{i,j=1}^{4} c_{ij} I_{ij}^{(1,2)}, \tag{3}$$

where we have adapted the results in Ref. [7]. The coefficients are

$$c_{ij} = g_1^2 N_{j1} N_{i1}^* (g_1 N_{j1} + g_2 N_{j2})(g_1 N_{i1}^* + g_2 N_{i2}^*), \tag{4}$$

where N_{ij} is the neutralino mixing matrix.

These three-body decays are typically mediated by the bino and, for Majorana neutralinos, are suppressed by its mass with $\Gamma_{\text{OSL}} \sim m_B^{-4}$ while $\Gamma_{\text{SSL}} \sim m_B^{-2}$. The bino mediated decays are partially responsible for the SSL excess over OSL in lepto-SUSY; see Fig. 2. For our sample point, where $m_{\tilde{\ell}_R}/m_{\tilde{\ell}_L} \simeq 0.44$, the SSL final state branching ratio is about 3.6 times that of OSL for both selectron and smuon three-body decays.

B. Higgses galore

Even though the decay of the heavier sleptons into the Higgs boson and the light sleptons is suppressed by the small Yukawa couplings, such decay is competitive with the three-body decay channels for the $\tilde{\mu}_2$, and it completely dominates for the $\tilde{\tau}_2$. Below, we derive the $\tilde{\tau}_2$ two-body decay widths into the Higgs and the Z bosons. Analogous results apply to the smuons. The mass eigenstates are defined as

$$\begin{pmatrix} \tilde{\tau}_1 \\ \tilde{\tau}_2 \end{pmatrix} = \begin{pmatrix} \cos\theta_{\tilde{\tau}} & \sin\theta_{\tilde{\tau}} \\ -\sin\theta_{\tilde{\tau}} & \cos\theta_{\tilde{\tau}} \end{pmatrix} \begin{pmatrix} \tilde{\tau}_R \\ \tilde{\tau}_L \end{pmatrix},$$

where $\theta_{\tilde{\tau}}$ is the mixing angle, $0 \le \theta_{\tilde{\tau}} < \pi$, and $m_{\tilde{\tau}_1} < m_{\tilde{\tau}_2}$. To the leading order,

$$\sin\theta_{\tilde{\tau}} \approx \frac{\mu m_\tau \tan\beta}{m_{\tilde{\tau}_2}^2 - m_{\tilde{\tau}_1}^2} \quad \text{and} \quad \cos\theta_{\tilde{\tau}} \approx 1. \tag{5}$$

The two-body decay widths are then

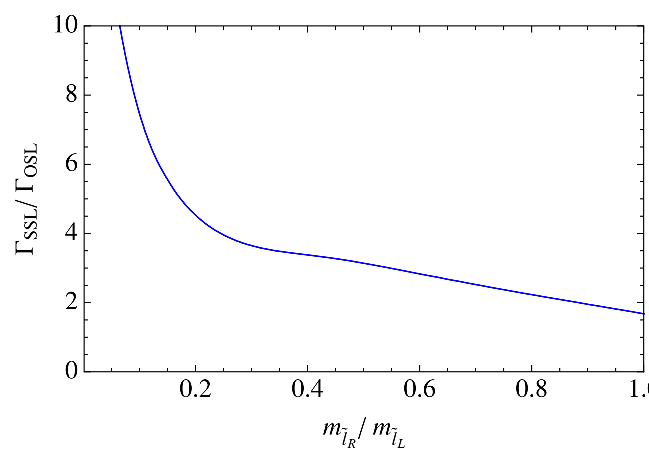

FIG. 2 (color online). $\Gamma_{\text{SSL}}/\Gamma_{\text{OSL}}$ ratio as a function of $m_{\tilde{\ell}_R}/m_{\tilde{\ell}_L}$. The neutralino mass matrix corresponds to our sample point.

$$\Gamma(\tilde{\tau}_2 \to \tilde{\tau}_1 + h) = \frac{\mu^2 y_\tau^2 \cos^2\alpha \cos^2(2\theta_{\tilde{\tau}})}{16\pi m_{\tilde{\tau}_2}} f_1(r_{\tilde{\tau}_1}, r_h),$$
$$\Gamma(\tilde{\tau}_2 \to \tilde{\tau}_1 + Z) = \frac{g_2^2 \sin^2(2\theta_{\tilde{\tau}}) m_{\tilde{\tau}_2}^3}{128\pi \cos^2\theta_W m_Z^2} f_2(r_{\tilde{\tau}_1}, r_Z), \tag{6}$$

where θ_W is the weak mixing angle, while the mass ratios are $r_{\tilde{\tau}_1} = m_{\tilde{\tau}_1}/m_{\tilde{\tau}_2}$ and $r_{h/Z} = m_{h/Z}/m_{\tilde{\tau}_2}$. The dimensionless functions f_1, f_2 are defined as

$$f_1(r_{\tilde{\tau}_1}, r_h) = \sqrt{\tfrac{1}{4}(1 - r_{\tilde{\tau}_1}^2 + r_h^2)^2 - r_h^2}, \tag{7}$$

$$f_2(r_{\tilde{\tau}_1}, r_Z) = ((1 - r_{\tilde{\tau}_1}^2)^2 - 2r_Z^2 - 2r_{\tilde{\tau}_1}^2 r_Z^2 + r_Z^4) f_1(r_{\tilde{\tau}_1}, r_Z). \tag{8}$$

In the decoupling limit, where $c_\alpha \sim s_\beta$, one finds that $\tan\beta$ drops out of the ratio of the two decay widths:

$$\frac{\Gamma(\tilde{\tau}_2 \to \tilde{\tau}_1 + Z)}{\Gamma(\tilde{\tau}_2 \to \tilde{\tau}_1 + h)} = \frac{((1 - r_{\tilde{\tau}_1}^2)^2 - 2r_Z^2 - 2r_{\tilde{\tau}_1}^2 r_Z^2 + r_Z^4)}{(1 - r_{\tilde{\tau}_1}^2)^2} \times \frac{f_1(r_{\tilde{\tau}_1}, r_Z)}{f_1(r_{\tilde{\tau}_1}, r_h)}. \tag{9}$$

For the sample spectrum we chose, $\tilde{\tau}_1$ decays into Higgses 53% of the time while for $\tilde{\mu}_1$, including three-body decays, the branching ratio to Higgses is 44%.

Below we provide some relevant branching ratios of other superparticles.

TABLE II. Branching ratios of squarks, neutralinos, and charginos.

Particle	Decay mode	Branching ratio
$\tilde{t}_1$	$\tilde{\chi}_1^0 t$	0.17
	$\tilde{\chi}_2^0 t$	0.24
	$\tilde{\chi}_3^0 t$	0.08
	$\tilde{\chi}_1^+ b$	0.50
$\tilde{t}_2$	$\tilde{\chi}_1^0 t$	0.32
	$\tilde{\chi}_2^0 t$	0.44
	$\tilde{\chi}_2^+ b$	0.07
$\tilde{u}_L$	$\tilde{\chi}_4^0 u$	0.29
	$\tilde{\chi}_2^+ d$	0.57
$\tilde{u}_R$	$\tilde{\chi}_1^0 u$	0.23
	$\tilde{\chi}_3^0 u$	0.76
$\tilde{\chi}_1^+$	$\tilde{\nu}\ell$	0.16
	$\tilde{\nu}_\tau \tau$	0.18
	$\tilde{\tau}_2 \nu_\tau$	0.61
$\tilde{\chi}_2^+$	$\tilde{\nu}\ell$	0.22
	$\tilde{\nu}_\tau \tau$	0.11
	$\tilde{\tau}_2 \nu_\tau$	0.11
$\tilde{\chi}_1^0$	$\tilde{\ell}_R \ell$	0.60
$\tilde{\chi}_3^0$	$\tilde{\ell}_R \ell$	0.56
	$\tilde{\ell}_L \ell$	0.06
$\tilde{\chi}_4^0$	$\tilde{\ell}_L \ell$	0.22

III. LHC PHENOMENOLOGY

Our analysis of collider signatures was performed using the following software tools. We generated the events at the parton level with the Monte Carlo generator MADGRAPH [12]. We used a modified version of BRIDGE [13] for particle decays to account for the $\tilde{\mu}_L - \tilde{\mu}_R$ mixing. Then, we passed the events through PYTHIA [14] to include showering-hadronization effects. Finally, we estimated the detector effects following the ATLFAST [15] approach. For example, to include energy resolution effects we modified the ATLFAST subroutines for the jet and electron energy smearing. The analysis of the events is performed with basic parton level η and p_T cuts on jets, leptons, and sleptons. We also imposed jet and lepton isolation cuts.

We focus on events characterized by

(1) large cross section production from squark pair production
(2) two hard jets (see Fig. 3 for the p_T distribution of jets from the squark decays)
(3) at least four leptonlike particles (leptons or stable sleptons).

We concentrated on these signals because they are practically background free. There are no sources of, real or fakes, four-lepton events with at least two SSL and two hard jets with the cross sections in the fb range (see the discussion in Sec. III C). Our goal is twofold. First, we want to show that statistically significant excesses of events can be observed with little integrated luminosity. Second, we want to demonstrate that mass reconstruction of several states is possible. In order to do that, we examine the events with four, five, or six leptonlike particles. Such events probe different decay cascades and are therefore sensitive to different intermediate states.

A. Sleptons or muons?

Long-lived sleptons are a promising feature of some of GMSB benchmark points [8,16,17]. In lepto-SUSY, the NLSP is a long-lived stau. Mass splittings between selectrons, smuons, and staus are rather small, so one cannot observe $\tilde{e}_R$ and $\tilde{\mu}_R$ decays. As we previously mentioned, the phenomenology will resemble the so-called "slepton co-NLSP scenario." A novel feature of lepto-SUSY is that pairs of sleptons are always accompanied by leptons. We presume the existing studies on long-lived sleptons in GMSB should be modified to account for high lepton multiplicity in this scenario, but we expect the essential features will remain unchanged.

Heavy, collider-stable particles appear as muons with a delayed arrival at the muon chambers. The dominant SM backgrounds are muons from the b and W decays. Cuts on the muon p_T and isolation requirements greatly reduce these backgrounds. To reduce the background from b decays, one applies cuts on the transverse momentum of typically $p_T > 50$ GeV [18]. On the other hand, in our case the slepton is detected in association with leptons. This will

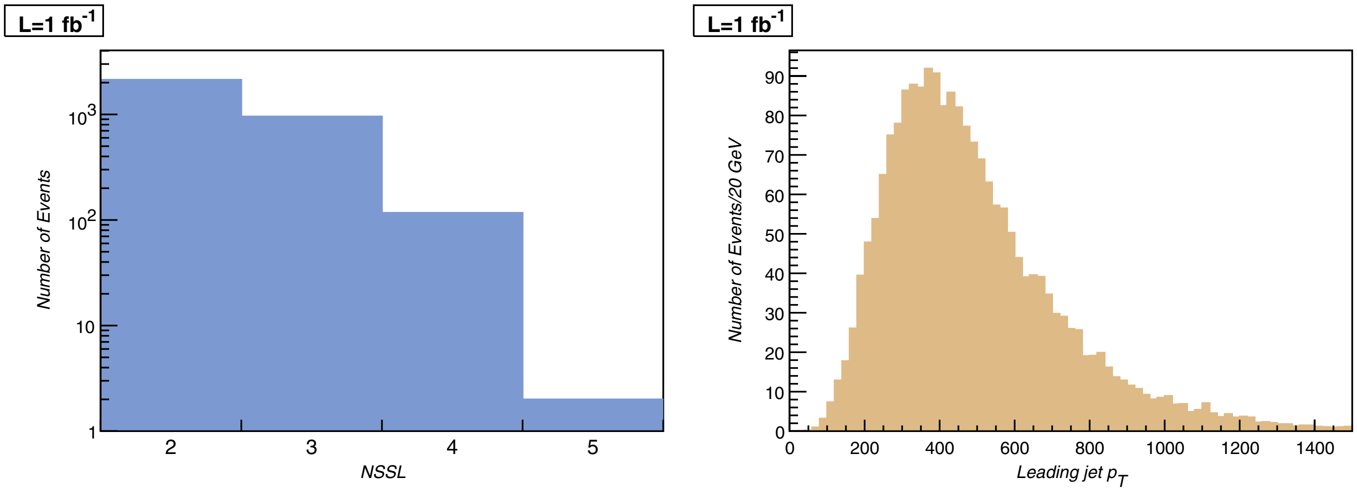

FIG. 3 (color online). Number of same-sign leptons and leading jet p_T distributions for $\sqrt{s} = 14$ TeV and $\mathcal{L} = 1$ fb^{-1}.

reduce b-decay backgrounds and a relaxed p_T cut is likely to suffice. Top decays have a higher p_T, but at the same time they have a smaller production cross section. The left plot in Fig. 4 shows the efficiency is high with a $p_T >$ 50 GeV cut.

For stable particles one can infer their mass by measuring the momentum and velocity. The momentum is measured with the tracker and the muon spectrometer. The velocity can be measured using two techniques: time of flight (TOF) from the muon system or using the ionization information from the silicon tracker [8,17]. Cosmic muons are the main background for the TOF technique. To reduce this background, TOF measurement is often correlated with an independent measurement of ionization in the tracker. At CMS, this approach is suitable for velocities $0.6 < \beta < 0.8$ [17]. Further refinements could be used to extend the range of β to about 0.9 [19]. At ATLAS, the TOF technique may be applicable up to β of around 0.95 [8].

Sleptons in lepto-SUSY are decay products of heavy squarks. Hence, the slepton β distribution is peaked towards large values. Indeed, most of our sleptons have velocities $\beta > 0.95$ and would therefore be likely misidentified as muons. To retain as much of the signal as possible, we treat the fastest sleptons with $\beta > 0.95$ as muons while we assume that the slower sleptons are properly identified. We also use the muon smearing, isolation, efficiencies, and charge misidentification parameters in the slepton analysis. Nevertheless, 30% (57%) of our sample contains at least one slepton with $\beta < 0.8$ (< 0.9) and an early slepton mass measurement is possible. Only 3% of the events contain 2 sleptons with velocities less than 0.8. In the dominant decay channels, as in the $2\ell + 2\tilde{\ell}_R + 2j$ channel, the total cross section of events with at least one slepton with $\beta < 0.9$ is approximately 150 fb.

Another challenge associated with slow-moving long-lived particles is the correct assignment of bunch crossing. The efficiency for assigning the correct bunch crossing for slow-moving particles decreases steeply with β. For $\beta \sim 0.8 - 1.0$, the efficiency is in the 80%–100% range, whereas for $\beta \sim 0.6$ it is only 15% [8]. A cut on the slepton $\beta > 0.8$ eliminates very little signal, as illustrated by the right plot in Fig. 4.

B. Production mechanism of lepto-SUSY

The main production mechanism for lepto-SUSY events is pair production of squarks

$$pp \rightarrow \tilde{q}\,\bar{\tilde{q}}, \tilde{q}\,\tilde{q}, \bar{\tilde{q}}\,\bar{\tilde{q}}$$

while the $pp \rightarrow \tilde{g}\,\tilde{q}$ channel is suppressed when gluinos are heavier than squarks; see Fig. 5. The cross sections for $pp \rightarrow \tilde{q}\,\bar{\tilde{q}}$ and $pp \rightarrow \tilde{q}\,\tilde{q}$ are of the same order for sparticle masses typical in lepto-SUSY. In the following study, production cross sections were computed using MADGRAPH [12] at the leading order and their sum is 2 pb. The cross sections obtained from MADGRAPH are compatible to those from PROSPINO with a k factor of $\mathcal{O}(1)$.

C. Four-lepton channels

Events with four leptonlike objects are best suited for reconstruction of masses of the initial colored and secondary color-neutral particles—squarks and neutralinos. We refer to electrons, muons, and sleptons as leptonlike particles no matter if the sleptons are correctly identified or not. The four-lepton events arise from short decay chains in which both neutralinos decay directly to heavy stable sleptons $\tilde{\ell}_R$ and leptons (that is e and μ only) as depicted in Fig. 6. Figure 6 also shows the muon and electron composition of the four-leptons events where muons include sleptons. Other diagrams could potentially *contaminate* this signal. For example, production of $\tilde{\chi}_4^0$ and $\tilde{\chi}_2^0$ neutralinos decaying into

$$\tilde{\chi}_4^0 \rightarrow 2\ell\tau\tilde{\tau}_R, \qquad \tilde{\chi}_2^0 \rightarrow \tau h\tilde{\tau}_R.$$

Since $\tilde{\chi}_4^0$ is winolike, it does not decay to $\tilde{\ell}_R$ directly but instead decays to $\tilde{\ell}_L$ and then to $\tilde{\ell}_R$. Those types of events occur at a lower rate than the signal we are interested in, therefore they do not pose a problem.

Events depicted in Fig. 6 do not have any missing energy hence cutting on $\not{E}_T$ would not affect our signal. Moreover, accurate missing energy calibration will be difficult in the early running, especially when hard jets are present in the event. Fortunately, we found that the selection of events in terms of the number of leptons is robust under different $\not{E}_T$ cuts. As a result, we do not impose a $\not{E}_T$ cut in our analysis of lepton channels. We will come back to the $\not{E}_T$ cut in the Higgs search discussion in Sec. III F.

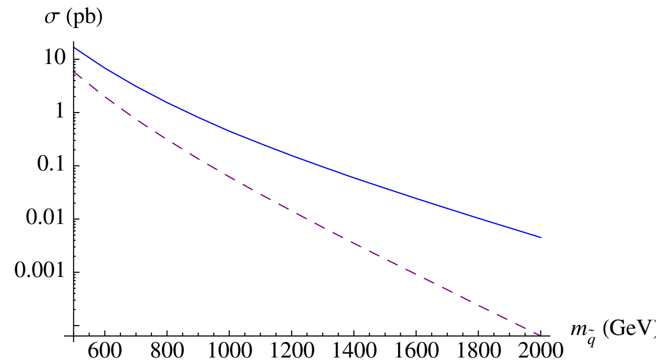

FIG. 5 (color online). The production cross sections $\sigma(pp \rightarrow \tilde{q}\,\bar{\tilde{q}} + \tilde{q}\,\tilde{q} + \bar{\tilde{q}}\,\bar{\tilde{q}})$ (solid blue line) and $\sigma(pp \rightarrow \tilde{q}\,\tilde{g})$ (dashed purple) at $\sqrt{s} = 14$ TeV for $m_{\tilde{g}}/m_{\tilde{q}} = 2$ using Prospino [20] at NLO.

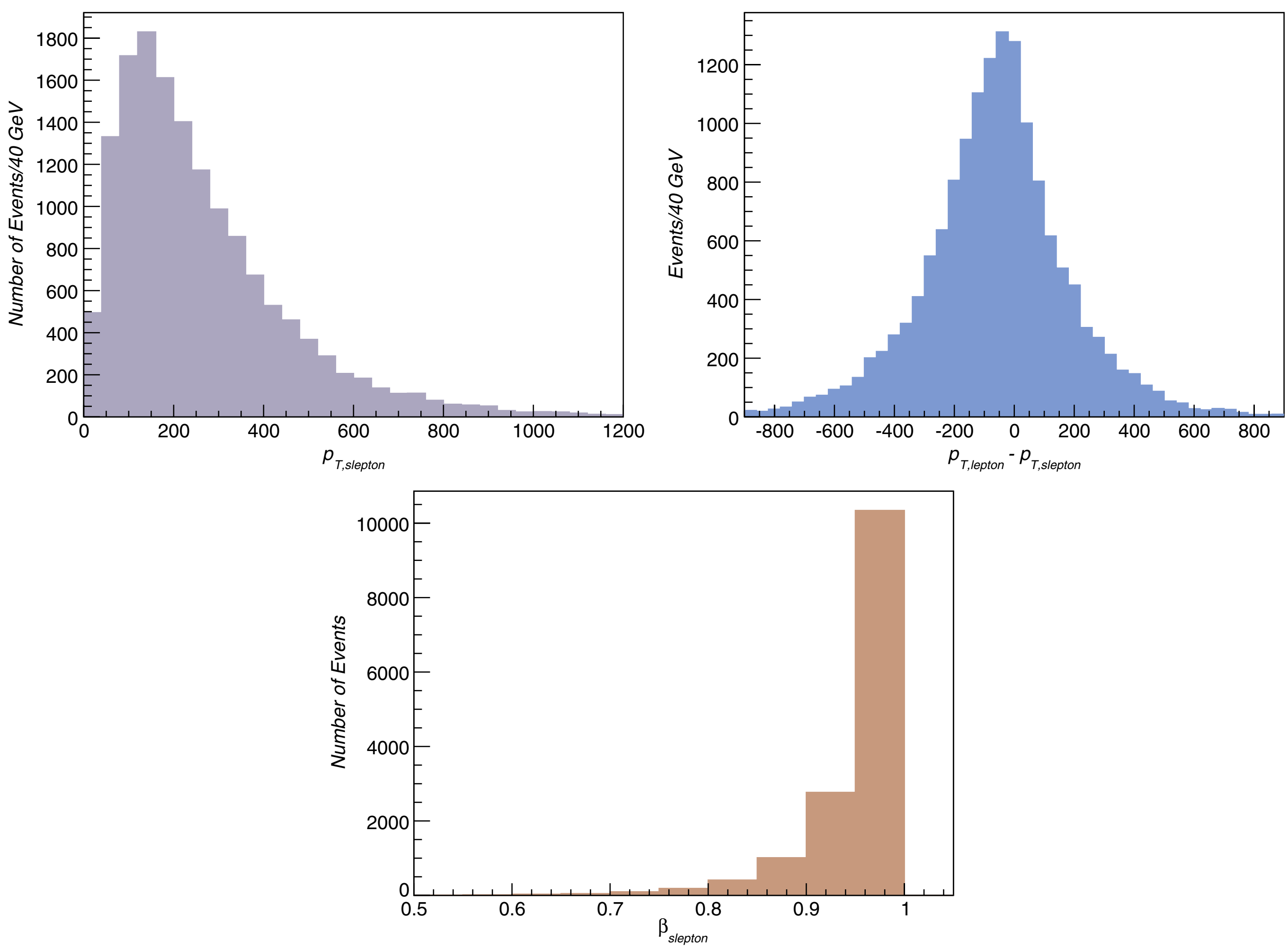

FIG. 4 (color online). Slepton p_T, lepton minus slepton p_T, and slepton velocity distributions assuming $\sqrt{s} = 14$ TeV and $\mathcal{L} = 10\ \text{fb}^{-1}$.

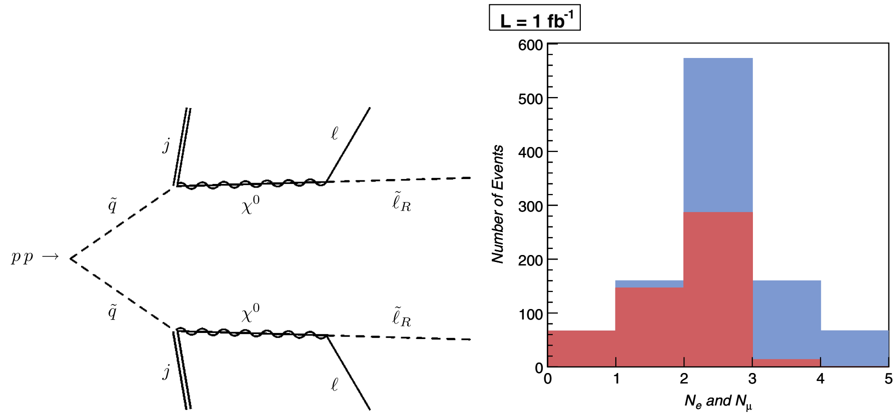

FIG. 6 (color online). Left panel: Four-lepton channels. Right panel: Electron (lower-red area) and muon (upper-blue area) composition of the four leptons.

We select four-lepton events using the following criteria

$$n_l = 4 \text{ (including sleptons) with } |\eta| < 2.5,$$
$$p_T > 10 \text{ GeV and parton level isolation cuts } \Delta R_{\ell\ell} > 0.4,$$
$$\Delta R_{\ell j} > 0.4, \quad n_j \geq 2 \text{ with } |\eta| < 2.5,$$
$$p_T > 15 \text{ GeV and post-PYTHIA isolation cuts } \Delta R_{jj} > 0.4. \tag{10}$$

With those cuts, the total cross section is 220 (690) fb for $\sqrt{s} = 10(14)$ TeV which corresponds to about 45 (140) events in 200 pb^{-1} of collected data. Notice very efficient hard cuts on the leading jets p_T can be applied; see Fig. 3. Efficiencies to identify leptons in the $|\eta| < 2.5$ are around 97% [8,17]. Those efficiencies are taken into account in the total cross sections we quote above.

There are sources of SM backgrounds for events with 4 leptons + 4 jets. After applying the cuts described in Eq. (10), we estimated all SM backgrounds are below the fb level. We generated the most important backgrounds with ALPGEN [21]: $t\bar{t}$ + jets, W + jets, WZ + jets, and QCD jets. Other SM backgrounds like ZZ + jets are tiny, even before we ask for a hard cut on the jets; see Fig. 3 in Ref. [21].

More relevant backgrounds come from QCD with jets faking leptons. We used a conservative estimate of 10^{-4} probability of that to happen [8]. Although QCD jets have a cross section of about 10^8 pb, requiring four fake leptons cuts down their rate to several orders of magnitude below 1 fb. Similar fake rate in backgrounds like W + jets or WZ + jets leads to a cross section significantly below the signal.

The $t\bar{t}$ + jets background has an initial cross section of about 1 nb. We estimated the b jets produce an isolated lepton in about 5×10^{-3}. For W decaying leptonically and the b's producing isolated leptons, we estimate a cross section of about 1 fb, which can be further reduced by applying a cut on the jets p_T.

Depending on whether sleptons are identified or not, we used different strategies to reconstruct the neutralinos participating in the diagram in Fig. 6. In the absence of SM background, combinatorial background is the main obstacle to the reconstruction.

Decay products of the squark decays are rather energetic—see Fig. 4—and tend to cluster. Objects coming from a common decay tend to be near each other in the ΔR parameter space. We used this information to reduce combinatorics. For the events with identified sleptons ($\beta \leq 0.95$), we paired a slepton with a nearby lepton through $\Delta R_{\ell\tilde{\ell}}$ selection. We followed the same procedure to pair the slepton-lepton pair with the nearest jet. For the events with sleptons misidentified as muons, we formed dilepton invariant masses and selected dilepton pairs with opposite charge and smaller $\Delta R_{\ell\tilde{\ell}}$. The ΔR discrimination is very powerful. Simply taking the average of pairing each lepton with any opposite-sign lepton would lead to no distinguishable features in the invariant mass distribution.

The slepton-lepton invariant mass distribution fully reconstructs the masses of three neutralinos $m_{\tilde{\chi}_1^0}$ and $m_{\tilde{\chi}_3^0}$. We have assumed that enough many slow sleptons are observed to establish the slepton mass. The left plot in Fig. 8 exhibits two clear peaks in $m_{\ell\tilde{\ell}}$ corresponding to $\tilde{\chi}_1^0$ and $\tilde{\chi}_3^0$. The slepton + lepton + jet reconstruction determines $m_{\tilde{q}}$; see Fig. 8. In Table II we present the Gaussian fits of the neutralinos and squark masses. On the other hand, for the misidentified sleptons, their energy is taken to be $|\vec{p}|$ where $\vec{p}$ is the three-momentum, which is smaller than their true energy $E = \sqrt{\vec{p}^2 + m^2}$. Therefore instead of peaks, the dilepton invariant mass distribution shows edge-like structure with end points at about $\sqrt{m_{\tilde{\chi}^0}^2 - m_{\tilde{\ell}_R}^2}$. Both the shift of the maximum and the smearing of the distribution, apparent on the right plot in Fig. 7, are the result of "missing mass." The slepton mass is not included in the calculations of energy whenever sleptons are misidentified.

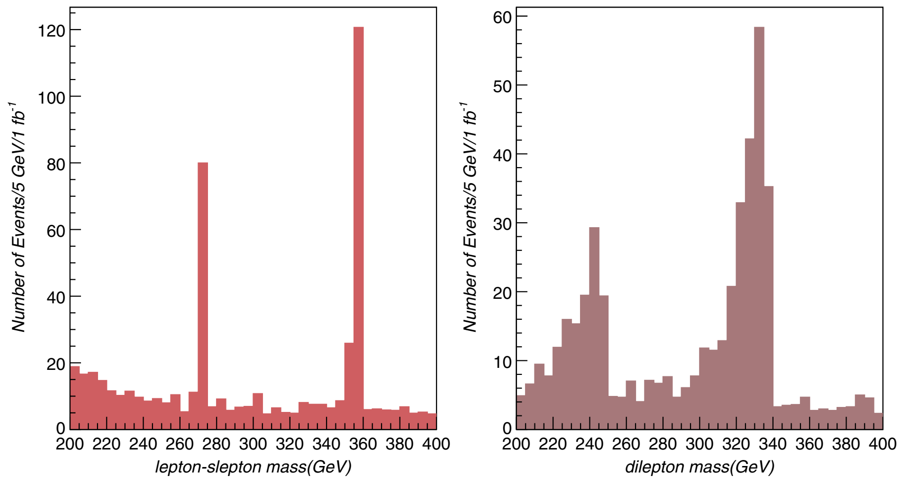

FIG. 7 (color online). Left panel: Neutralino reconstruction from slepton-lepton invariant mass for $\sqrt{s} = 14$ TeV and $\mathcal{L} = 1\,\mathrm{fb}^{-1}$. Right panel: Dilepton invariant mass distribution.

Finally, the difference in ΔR distribution between the chosen dilepton and the wrong dilepton combination is apparent in Figure 8—*correct* pairings have lower $\Delta R_{\ell\ell}$.

D. Five-lepton channels

The five-lepton channels, like the ones depicted in Fig. 9, have a long decay chain involving $\tilde{\chi}^{\pm}$ decaying to $\tilde{\ell}_L$ or $\tilde{\nu}$. Figure 9 also shows the muon and electron composition of the five leptons. We use this channel mostly for $\tilde{\ell}_L$ mass reconstruction as well as for gaining a less accurate estimate of the $\tilde{\nu}_L$ and $\tilde{\chi}^{\pm}$ masses.

Events in the five-lepton channel are selected with cuts similar to those used in four-lepton analysis and described in Eq. (10), except now $n_\ell = 5$. The total cross section of this channel is 137 (426) fb at $\sqrt{s} = 10(14)$ TeV and gives 27 (426) events at 0.2(1) fb^{-1}.

For reconstruction, we selected slepton-lepton pairs with smaller $\Delta R_{\ell\tilde{\ell}}$ and then formed slepton + 2 lepton clusters by adding to the slepton-lepton pair another nearby lepton chosen through ΔR selection. The decay $\tilde{\ell}_L \to 2\ell + \tilde{\ell}_R$ can be fully reconstructed by the slepton + 2 lepton lepton invariant mass. The distribution in Fig. 11 shows a resonance peak at the $\tilde{\ell}_L$ mass, fitted to be 252 GeV (see Table II).

The $\tilde{\nu}$ and $\tilde{\chi}^{\pm}$ cannot be fully reconstructed as their decays involve missing energy. Instead, we define the transverse mass variables of the system:

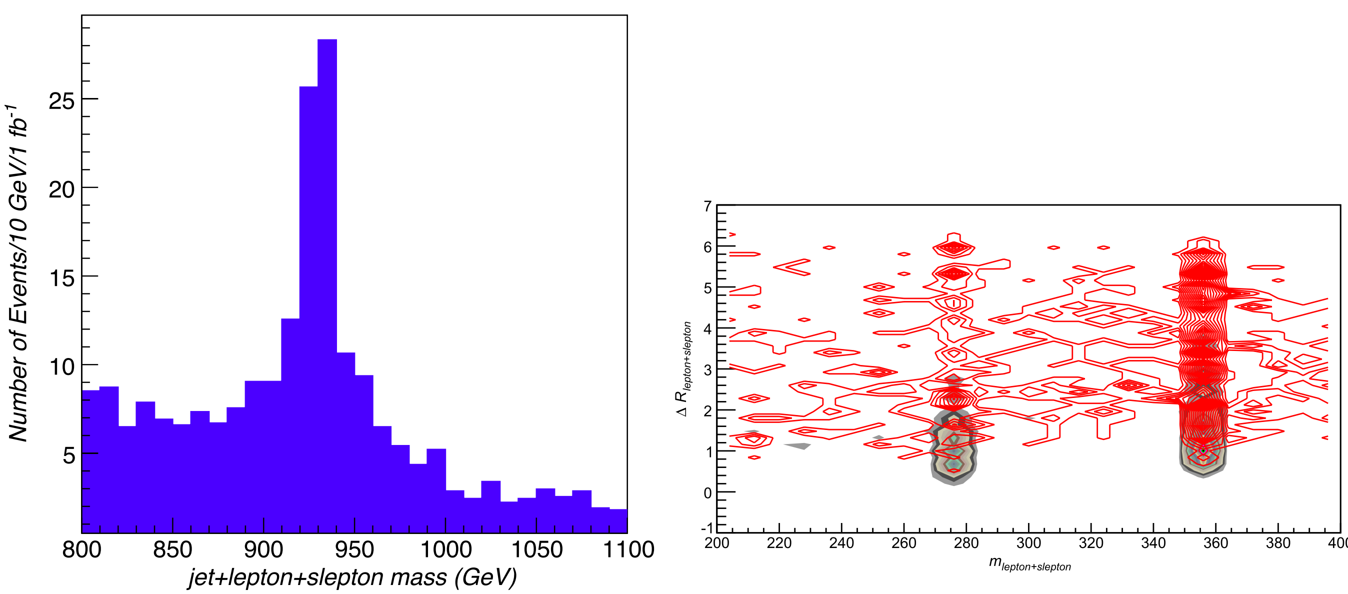

FIG. 8 (color online). Left panel: Squark reconstruction for $\sqrt{s} = 14$ TeV and $\mathcal{L} = 1$ fb^{-1}. Right panel: ΔR distribution for the chosen pair (in the lower contour lines) and the rejected pair (in the higher red lines).

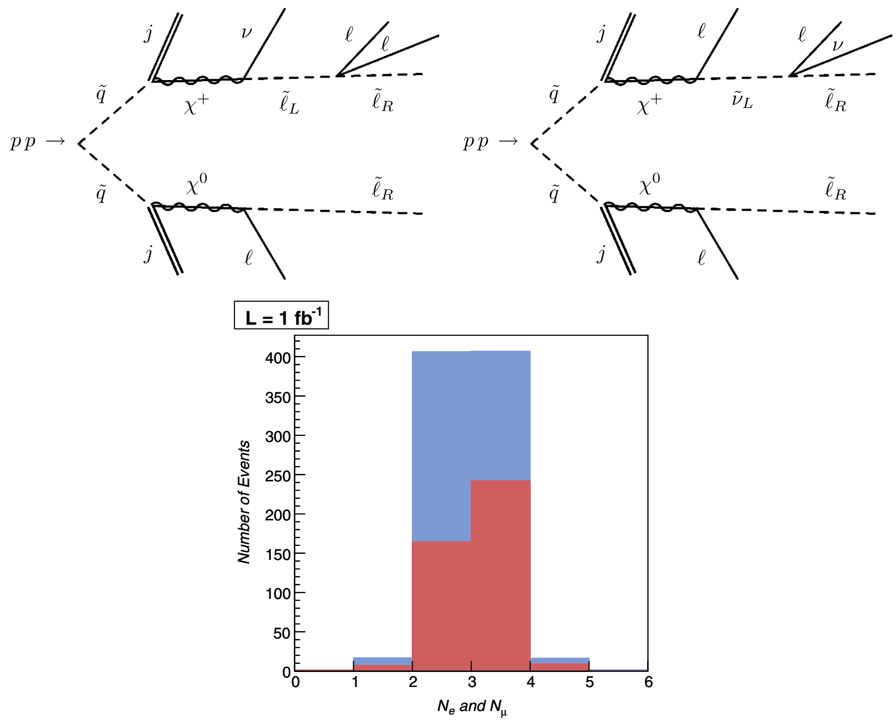

FIG. 9 (color online). Upper panel: Five-lepton channels. Lower panel: Electron (lower-red area) and muon (upper-blue area) composition of the five leptons.

$$M_{iT}^2 = (E_{iT} + \not{E}_T)^2 - (\vec{p}_{iT} + \not{p}_T)^2, \tag{11}$$

where i is either slepton-lepton or slepton + two leptons. We cannot estimate $\not{E}_T$ miscalibration in the early running, and the information obtained from transverse mass, as in Fig. 11, very much depends on how accurate the achieved calibration will be.

The missing energy measured by the calorimeter, Fig. 10, is small and is mostly below 100 GeV. Conservatively, we impose no missing energy cut since selection on the number of leptons is sufficient to reduce backgrounds. Figure 10 also shows the contours in the $(\not{E}_T, M_{\tilde{\ell}+2\ell T})$ plane. The contours are the most dense around $\not{E}_T \sim 30$ GeV, $M_{\tilde{\ell}+2\ell T} \sim 300$ GeV corresponding to the $\tilde{\chi}_1^{\pm}$. Because the missing energy comes solely from the single neutrino produced by either $\tilde{\nu}$ or $\tilde{\chi}^{\pm}$ decay, one expects to see Jacobian edges at $M_{\tilde{\ell}+\ell T} \sim M_{\tilde{\nu}}$ and at $M_{\tilde{\ell}+2\ell T} \sim M_{\tilde{\chi}^{\pm}}$. The plots in Fig. 11 depict an edge at the sneutrino mass 236 GeV in the slepton-lepton transverse mass distribution and two edges at the chargino masses 294 GeV and 677 GeV in the slepton + 2 lepton transverse mass distribution.

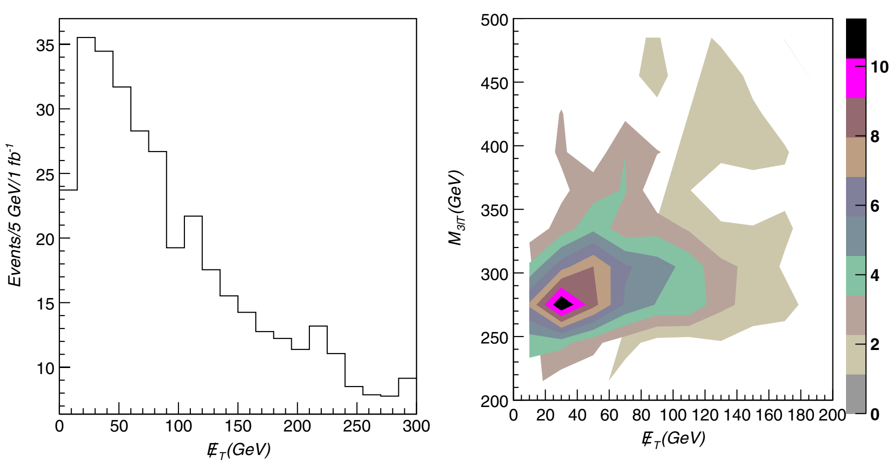

FIG. 10 (color online). $\not{E}_T$ distribution and $(\not{E}_T, M_T)$ distribution.

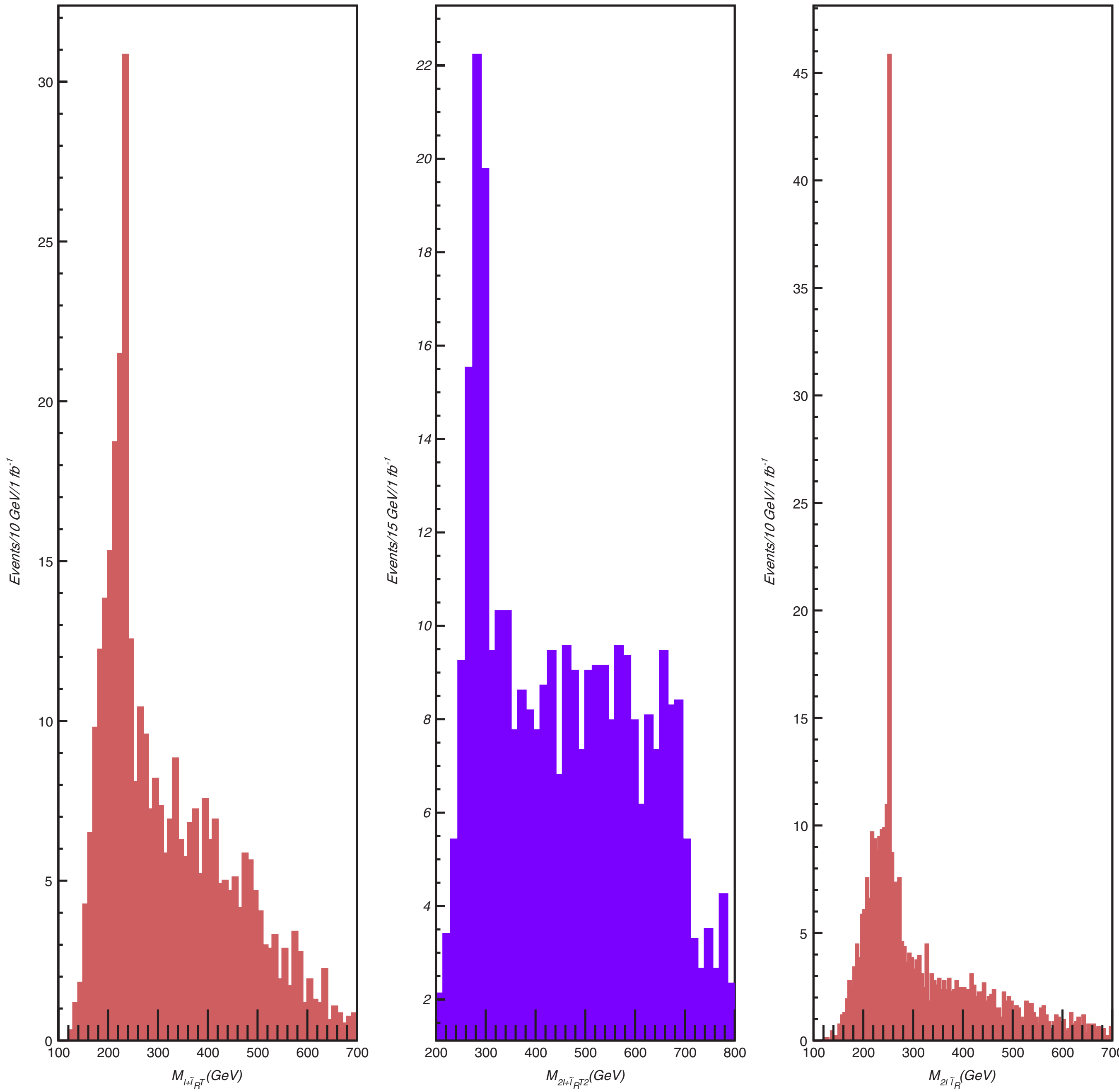

FIG. 11 (color online). Chargino-sneutrino transverse mass, slepton invariant mass reconstruction for $\sqrt{s} = 14$ TeV and $\mathcal{L} = 1\ \mathrm{fb}^{-1}$.

E. Six-lepton channels

Channels with six leptons and no missing energy arise mostly from the combination of two types of cascades

$$\text{short:}\ \tilde{\chi}^0 \to \tilde{\ell}_R \ell, \tag{12}$$

$$\text{long:}\ \tilde{\chi}^0 \to \tilde{\ell}_L \ell \to \tilde{\ell}'_R \ell' 2\ell. \tag{13}$$

In terms of the branching ratios, the dominant cascades are combinations of the long (L) and short (S) cascades. The (S,L) cascade combination originates from the following gauginos

$$(\tilde{\chi}^0_{1,3}, \tilde{\chi}^0_3), \qquad (\tilde{\chi}^0_{1,3}, \tilde{\chi}^0_4), \qquad (\tilde{\chi}^0_2, \tilde{\chi}^0_3), \qquad (\tilde{\chi}^0_2, \tilde{\chi}^0_4), \tag{14}$$

which are ordered by the total production rate from the highest to lowest. The first neutralino in any bracket yields a short cascade, while the second neutralino a long one.

There are also some (L,L) combinations producing six leptons and no missing energy, where a tau is identified as a jet. Among those, only one combination $(\tilde{\chi}_4, \tilde{\chi}_4)$ is produced at a comparable rate to that of $(\tilde{\chi}_2^0, \tilde{\chi}_3^0)$, which itself is very rare. Therefore, our signal mostly comes from a combination of the (S,L) cascades.

Events in the six-lepton channel are selected with cuts similar to the ones described in Eq. (10), except now $n_\ell = 6$. The muon and electron composition of the six leptons is shown in Fig. 12. The total cross section of this channel is 70 (225) fb at $\sqrt{s} = 10(14)$ TeV and gives 14 (225) events at 0.2(1) fb^{-1}. The slepton-lepton invariant mass would reconstruct the neutralino of the short chain with a contamination from partially reconstructing the $\tilde{\ell}_L$ of the long chain; see Fig. 13. Those neutralinos were already reconstructed in the four-lepton case with better statistics in that channel.

The slepton + 2 lepton invariant mass would reconstruct the long chain three-body decay originating from $\tilde{\ell}_L$. The peak corresponding to the slepton mass is clearly visible in Fig. 13.

Using again the ΔR selection, one can pair the combination of the slepton + 2 lepton and nearby lepton from the long cascade. The long cascades reconstruct mostly the $\tilde{\chi}_3^0$ and $\tilde{\chi}_4^0$ since these neutralinos are the most likely ones to originate the long cascades, as described in Eq. (14). Figure 13 shows clearly the peaks for the $\tilde{\chi}_{3,4}^0$ neutralinos. In Table II we quote the Gaussian fit for the $\tilde{\chi}_4^0$ mass.

Finally, we can pair the neutralino reconstruction with the nearby (in ΔR) leading jet. One can use either the long or the short combination. The squark reconstruction is similar to the four-lepton case but with lower statistics, hence we do not present it here.

F. Discovery of the Higgs

As in any MSSM model, the SM-like Higgs boson in lepto-SUSY is too light to decay into two W bosons. The Higgs then decays predominantly into $b\bar{b}$ with a branching ratio of about 80%. Because of large backgrounds, the Higgs searches at low mass are focused on a rarer but cleaner decay, $h \to \gamma\gamma$, which greatly limits their statistics.

In lepto-SUSY, in contrast to common-lore Higgs searches, the Higgs discovery channel is $h \to b\bar{b}$. Because the Higgs is produced in cascade decays it is free of SM backgrounds (see discussion in Sec. III C for details on SM backgrounds). It is therefore possible to discover h through the analysis of a clean $b\bar{b}$ invariant mass distribution. The relevant decay chain is illustrated in Fig. 14.

Energetic jets, including b jets, are produced in the final state in several ways, not only through the decay of the Higgs boson. For example, $\tilde{\mu}_2$ or $\tilde{\tau}_2$ at the end of the chain can decay to the Z, which in turn can decay to $b\bar{b}$. For our sample point, we found that the decays to h are competitive with the decays to Z, with branching ratios:

$$\mathrm{BR}\,(\tilde{\mu}_1 \to h(Z) + \tilde{\mu}_2) = 44.1\% \qquad (35.1\%) \tag{15}$$

$$\mathrm{BR}\,(\tilde{\tau}_1 \to h(Z) + \tilde{\tau}_2) = 53.3\% \qquad (46.6\%). \tag{16}$$

The Higgs and Z are decayed inside PYTHIA [14].

To reconstruct the Higgs mass, we selected events characterized by

$$\begin{gathered} n_l \leq 4 \quad \text{with} \quad |\eta| < 2.5, \\ p_T > 10 \text{ GeV and parton level isolation cuts } \Delta R_{\ell\ell} > 0.4, \\ \Delta R_{\ell j} > 0.4, \qquad n_j \geq 4 \quad \text{with} \qquad |\eta| < 2.5, \qquad p_T > 15 \text{ GeV}, \\ p_{T,j_1} - p_{T,j_4} > 300 \text{ GeV and post-PYTHIA isolation cuts } \Delta R_{jj} > 0.4. \end{gathered} \tag{17}$$

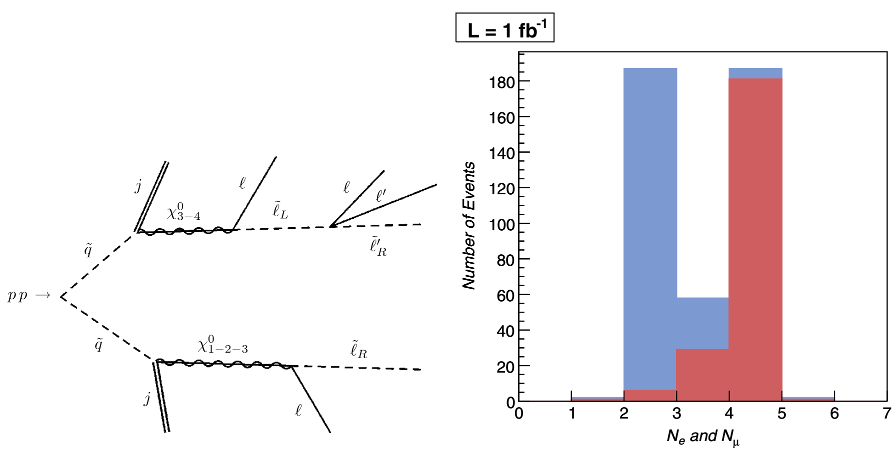

FIG. 12 (color online). Left panel: Six-lepton channel. Right panel: Electron (lower-red area) and muon (upper-blue area) composition of the six leptons.

We ordered the jets according to decreasing p_T. With no b tagging, we assume the third and fourth jets come from the end of the decay chain and therefore are the b jets we are interested in. We then construct dijet invariant mass of the third and fourth leading jets to reconstruct the Z and Higgs masses. In Fig. 15, the Z and Higgs peaks are clearly visible with bin size of 10 GeV. In Fig. 16, we show how relaxing the $\not{E}_T$ cut slowly introduces more combinatorics but still retains proportionately the Z and h signals. We chose a cut $\not{E}_T < 40$ GeV, which we consider a conservative choice for early running. The total cross section for those events is 100 (320) fb at 10 (14) TeV, which leads to about 20 events in the 200 pb^{-1} run at 10 TeV.

We can use rough cuts on the invariant mass to estimate the significance of these events. With 1 fb^{-1} of data, there are 50 events for $m_{\rm dijet}$ between 60 and 100 GeV and 37 events between 100 and 130 GeV. But that counting does not take into account two important facts. First, the Z and h peaks overlap. We used Gaussian fits to estimate that the Higgs peak contains 51 events and the Z contamination under the h Gaussian is 16 events, leading to 35 Higgs events at 1 fb^{-1}; see Table III for details. The second

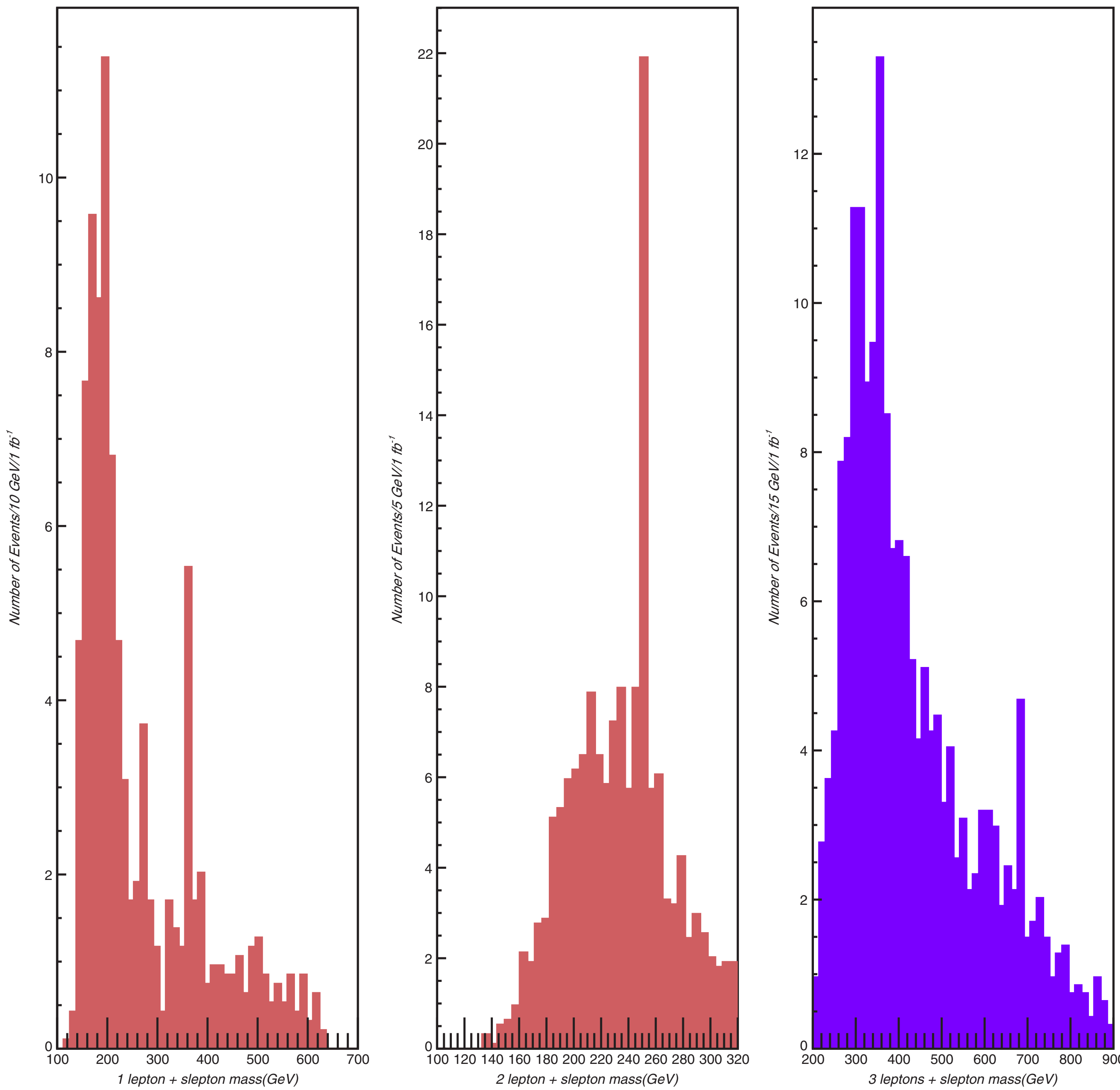

FIG. 13 (color online). Six-lepton channel invariant mass distributions for $\sqrt{s} = 14$ TeV and $\mathcal{L} = 1$ fb^{-1}.

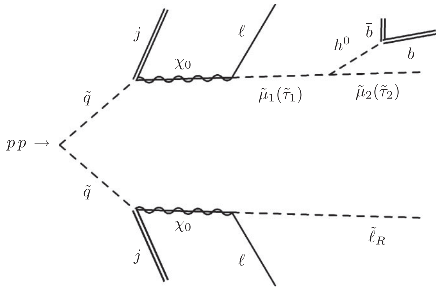

FIG. 14. Relevant process for Higgs mass reconstruction.

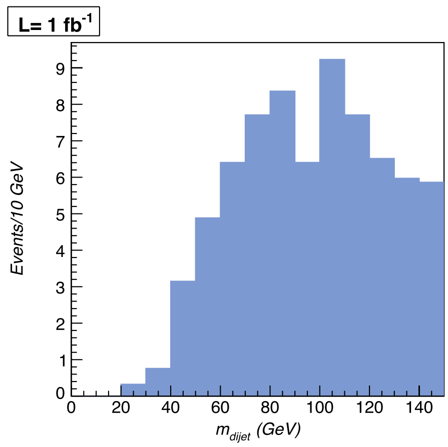

FIG. 15 (color online). Invariant dijet mass distribution with $\not{E}_T < 40$ GeV without b tagging for $\sqrt{s} = 14$ TeV and $\mathcal{L} = 1\ \mathrm{fb}^{-1}$.

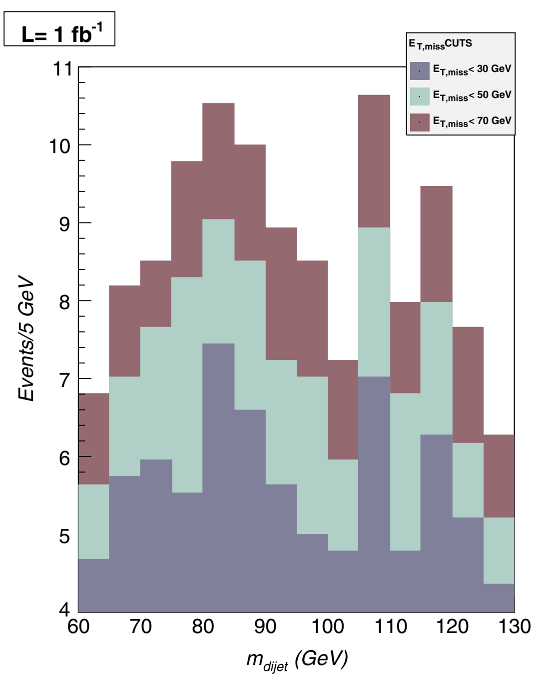

FIG. 16 (color online). Invariant dijet mass distribution for $\sqrt{s} = 14$ TeV and $\mathcal{L} = 1\ \mathrm{fb}^{-1}$ and different $\not{E}_T$ cuts.

TABLE III. Gaussian fits of the peak signals for $\sqrt{s} = 14$ TeV and $\mathcal{L} = 1\ \mathrm{fb}^{-1}$. The last column refers to the number of leptons in the channel. For $\sqrt{s} = 10$ TeV and $\mathcal{L} = 0.2\ \mathrm{fb}^{-1}$, each channel event rate is reduced by a factor of 13.

	Mass (GeV)	Width (GeV)	Events	Channel
$\tilde{\chi}_1^0$	272	2	96	4
$\tilde{\chi}_3^0$	356	2	132	4
$\tilde{q}$	930	11	83	4
$\tilde{\ell}_L$	252	3	68	5
$\tilde{\chi}_4^0$	680	10	7	6

important effect is the combinatorial background which lies below the two peaks, and extended in a larger range of dijet masses. The combinatorial background increases by relaxing the $\not{E}_T$ cut and could be fitted with a parabola or a Gaussian. Our conclusion is that a proper treatment of the combinatorial background would require full simulation.

G. Dirac or Majorana gauginos

Lepto-SUSY spectrum can arise in models that contain an approximate $U(1)_R$ symmetry, making Dirac gaugino masses necessary. Using the clean lepto-SUSY channels, it is straightforward to distinguish the Majorana or Dirac nature of the neutralinos. For example, a Dirac gluino forbids squark pair production channels, like $pp \rightarrow \tilde{q}\,\tilde{q}$, while $pp \rightarrow \tilde{q}\,\bar{\tilde{q}}$ is allowed [3,22]. In the cleanest four-lepton final state in lepto-SUSY we have simulated, the selected events have both same-sign and opposite-sign leptons. By simple combinatorics, both configurations have the same probabilities. In the Dirac gaugino case, only the opposite-sign lepton configuration remains. The lepton charge distribution gives a straightforward discriminant of the two types of gaugino soft mass.

IV. MODELS WITH LEPTO-SUSY SPECTRUM

In this section we propose a model-independent parametrization of the lepto-SUSY soft mass terms and discuss models that lead to lepto-SUSY spectra. Our parametrization is general, but it is most useful for models in which the supersymmetry mediation mechanism involves gauge interactions.

We parametrize the soft mass terms assuming that various superpartners acquire soft mass contributions proportional to their SM gauge charges. The scalar masses pick up contributions from every gauge interaction they participate in, where each gauge group is characterized by the corresponding coefficient K_i

$$\tilde{m}^2(R) = \sum_{i=1}^{3} C_2(R_i) K_i, \tag{18}$$

where the sum runs over the SM gauge groups and the quadratic Casimir, C_2, is $(N^2 - 1)/2N$ for an $SU(N)$ fundamental representation while it is $3/5$ times the hypercharge squared for $U(1)$. The R_i denote the representations of the field under the corresponding SM gauge groups. Finally, the coefficient's K_i's encode the details of the particular supersymmetry breaking mechanism in play,

$$K_i = \frac{\alpha_i}{\pi} m_i^2 n_i^2 \qquad (i = 1, 2, 3), \tag{19}$$

where m_i are the gaugino masses.

With unspecified dimensionless n_i's, this parametrization is still completely general subject only to the assumption in Eq. (18). In specific models, like GMSB [2] with a large number of messengers or L$\tilde{g}$M [1] (see also [23,24]), it turns out that the parameters n_i are $\mathcal{O}(1\text{–}10)$ numbers. Our parametrization stresses the fact that scalar soft mass squared is typically one-loop suppressed compared to the corresponding gaugino masses squared in such models. The squares of the parameters n_i are smaller than the loop suppression and therefore the scalar soft masses are smaller, by a factor of a few, than the gaugino masses.

One additional parameter needs to be introduced in the Higgs sector. According to Eq. (18), $m_{H_d}^2$ and $m_{H_u}^2$ are both positive. Typically, EWSB is triggered by additional contributions to $m_{H_u}^2$ induced by the large value of the top quark Yukawa coupling. We incorporate such a contribution as a free parameter n_4:

$$\delta \equiv -m_{H_d}^2 + m_{H_u}^2 = -\frac{\alpha_3 \lambda_t^2}{4\pi^3} m_3^2 n_4^2. \tag{20}$$

We also assume that the gaugino masses obey the unified relations, that is $m_i \propto \alpha_i$. In summary, our parameter space is defined by an overall scale, given by the gluino mass, four dimensionless parameters which parametrize the details of SUSY-breaking mechanism, $\tan\beta$, and $\mathrm{sign}\mu$:

$$m_3, \qquad n_i (i = 1, 2, 3, 4), \qquad \tan\beta, \qquad \mathrm{sign}\mu. \tag{21}$$

We neglect the trilinear A-terms as they tend to be small in the GMSB and L$\tilde{g}$M. As we discussed earlier, the A-terms would have to be unnaturally large to make a sizable impact on the mass spectrum.

In Sec. II we discussed the lepto-SUSY spectrum and constraints on the spectrum. In terms of our parametrization, the mass ranges in Eq. (1), correspond to

Parameter	Range
n_1	[2, 5]
n_2	[0.5, 6]
n_3	>1.8
n_4	>1.75

Therefore, lepto-SUSY spectra are obtained for $\mathcal{O}(1)$ parameters. For example, the sample spectrum presented in Table I is obtained from the input parameters in Table IV.

The parameters n_i are $\mathcal{O}(1)$ numbers in models where there is a suppression of the squark and slepton masses compared to the gaugino masses of order of a loop factor. For illustration, we briefly examine how such $\mathcal{O}(1)$ values of n_i arise in some models.

TABLE IV. Fits of the Z and h peaks with $\not{E}_T < 40$ GeV, for $\sqrt{s} = 14$ TeV and $\mathcal{L} = 1\ \mathrm{fb}^{-1}$.

	Mass (GeV)	Width (GeV)	Events
Z	82	23	82
h	113	15	51

In GMSB, the gaugino masses are generated at one-loop level, while the scalar masses squared at two loops. Both the gaugino and scalar masses squared are proportional to the number of messengers, N_m. Parametrically

$$n_i \propto \frac{1}{\sqrt{N_m}} \sqrt{\frac{\pi}{\alpha_i}}, \tag{22}$$

that is one obtains lepto-SUSY spectrum when the number of messengers is of order of the loop suppression factors. The above equation holds for n_4 as well since soft Higgs masses are generated at the next loop order compared to the scalar masses.

In gaugino mediation [25], the scalar masses are generated radiatively through diagrams involving the gauginos. Whether or not the scalar masses are suppressed compared to the gauginos depends on the mediation scale. In high-scale models [26], the natural one-loop suppression is compensated for by large logarithm of the ratio of the mediation scale to the weak scale. In L$\tilde{g}$M one naturally obtains $n_i \approx 1$. The $m_{H_d}^2 - m_{H_u}^2$ mass splitting, parametrized by n_4, is generated by two-loop diagrams involving the stop and is of order indicated in Eq. (20).

Another example of models with lepto-SUSY spectra are models with supersoft SUSY breaking [3]. In such models, SUSY breaking is caused by a D-term vacuum expectation value in a new $U(1)$ gauge sector. Because of unbroken R symmetry the gaugino masses are necessarily Dirac type. The SUSY-breaking D-term couples to the visible sector through higher dimensional operators. The lowest dimensional operator responsible for gaugino masses is a dimension five operator, while the operator responsible for scalar masses is of dimension ten. The suppression of the scalar masses compared to that of the gauginos is therefore natural for such models. Dirac or Majorana gaugino masses can be easily distinguished using charge asymmetries as explained in Sec. III G.

V. CONCLUSION AND OUTLOOK

Lepto-SUSY is a well-motivated supersymmetric scenario. The ordering of the spectrum ensures, due to kinematics alone, copious lepton production in decay chains. Therefore, the signals are very clean and the LHC has a tremendous discovery potential. Another interesting feature is that the Higgs boson is produced in SUSY cascade decays, which reduce the background so much that the Higgs can be discovered via the $b\bar{b}$ channel.

We studied a sample spectrum of lepto-SUSY and estimated the LHC potential of discovering and reconstructing this type of spectrum. The discovery channels have cross sections governed by the QCD production of squarks and are characterized by two hard jets, two collider-stable sleptons, and at least two leptons. If the sleptons are misidentified as muons, which is likely, the signatures are four or more leptons and two hard jets. A discovery of the stable slepton is possible in the early running of the LHC. Lepto-SUSY with 1 TeV squarks generates sleptons with velocities $0.6 < \beta < 0.8(0.9)$ at a rate of 210 (400) fb at 10 TeV, resulting in 40 (80) stable sleptons with 200 pb^{-1} of data.

The Higgs discovery channel is through the $h \to b\bar{b}$ decay in association with four leptons and two hard jets. We estimate the prospects for Higgs discovery are good with less than 1 fb^{-1} of data at 14 TeV, again assuming 1 TeV squarks.

Using the four-lepton channel one can determine the squark masses and all neutralinos, except the second Higgsino and wino, in the 10 TeV run with 200 pb^{-1} of data. In the five-lepton channel—which is the only $\not{E}_T$ channel—one could further determine the masses of the sneutrino, heavy slepton, and charginos using the transverse mass variables. The six-lepton channel has a smaller branching ratio, but it will allow one to determine the wino mass with just 1 fb^{-1} of data during the 14 TeV run.

There are several directions worth pursuing in the context of lepto-SUSY. The light Higgs is produced in a clean environment, so one may attempt to use it for an extraction of the bottom Yukawa coupling. We only studied the light Higgs, but there may be new ways to discover the remaining Higgs bosons in lepto-SUSY. We did not investigate how changing the spectrum, by altering various mass ratios, affects the signatures of interest. For instance, increasing the squark-gluino mass ratio can enhance the squark-gluino associated production, which in turn, may offer new signatures and, of course, prospects for the gluino mass measurement. We have not fully exploited the flavor information in our analysis. Since the collider-stable sleptons will often be misidentified as muons one could take advantage of this fact to refine the analysis. Last but not least, for the channels with $\not{E}_T$ one could use more sophisticated kinematic variables to improve the sensitivity.

ACKNOWLEDGMENTS

We thank Martin Schmaltz for collaboration in the early stages of this work and useful suggestions. We would like to thank Ketevi Assamagan, Tulika Bose, and Adam Martin for their comments and suggestions. We also thank Steve Martin for pointing out an error in an earlier version of this analysis. The work of A. D. S. is supported in part by INFN and in part by the US Department of Energy (DOE) under Contract No. DE-FG02-05ER41360. J. F. and W. S. are supported in part by the DOE under Grant No. DE-FG-02-92ER40704, while V. S. is supported under Grant No. DE-FG02-91ER40676. V. S. and W. S. would like to thank the Aspen Center of Physics, where part of this work was done.

[1] A. De Simone, J. Fan, M. Schmaltz, and W. Skiba, Phys. Rev. D **78**, 095010 (2008).
[2] G. F. Giudice and R. Rattazzi, Phys. Rep. **322**, 419 (1999).
[3] P. J. Fox, A. E. Nelson, and N. Weiner, J. High Energy Phys. 08 (2002) 035; A. E. Nelson, N. Rius, V. Sanz, and M. Unsal, J. High Energy Phys. 08 (2002) 039; Z. Chacko, P. J. Fox, and H. Murayama, Nucl. Phys. **B706**, 53 (2005).
[4] J. Abdallah *et al.* (DELPHI Collaboration), Eur. Phys. J. C **27**, 153 (2003).
[5] A. Djouadi, M. M. Muhlleitner, and M. Spira, Acta Phys. Pol. B **38**, 635 (2007); A. Djouadi, J. L. Kneur, and G. Moultaka, Comput. Phys. Commun. **176**, 426 (2007).
[6] S. P. Martin, arXiv:hep-ph/9709356; T. Plehn, arXiv:0810.2281; B. C. Allanach, Eur. Phys. J. C **59**, 427 (2009).
[7] S. Ambrosanio, G. D. Kribs, and S. P. Martin, Nucl. Phys. **B516**, 55 (1998).
[8] ATLAS Collaboration, "ATLAS detector and physics performance," Technical Design Report Vol. 2, arXiv:0901.0512; Report No. CERN-OPEN-2008-020.
[9] S. Ambrosanio *et al.*, arXiv:hep-ph/0002191; S. Dimopoulos, S. D. Thomas, and J. D. Wells, Nucl. Phys. **B488**, 39 (1997); S. Dimopoulos *et al.*, Nucl. Phys. B, Proc. Suppl. **52**, 38 (1997); S. Dimopoulos, M. Dine, S. Raby, and S. D. Thomas, Phys. Rev. Lett. **76**, 3494 (1996).
[10] J. R. Ellis, A. R. Raklev, and O. K. Oye, J. High Energy Phys. 10 (2006) 061.
[11] H. E. Haber and G. L. Kane, Phys. Rep. **117**, 75 (1985).
[12] F. Maltoni and T. Stelzer, J. High Energy Phys. 02 (2003) 027.
[13] P. Meade and M. Reece, arXiv:hep-ph/0703031.
[14] T. Sjostrand, S. Mrenna, and P. Skands, J. High Energy Phys. 05 (2006) 026.
[15] ALTFAST documentation (https://twiki.cern.ch/twiki/bin/view/Atlas/AtlfastDocumentation).
[16] M. Fairbairn *et al.*, Phys. Rep. **438**, 1 (2007).
[17] G. L. Bayatian *et al.* (CMS Collaboration), J. Phys. G **34**, 995 (2007).
[18] B. C. Allanach *et al.*, J. High Energy Phys. 08 (2001) 051; S. Ambrosanio *et al.*, arXiv:hep-ph/0012192; S. Ambrosanio *et al.*, J. High Energy Phys. 01 (2001) 014.
[19] T. Bose (private communication).
[20] W. Beenakker, R. Hopker, and M. Spira, arXiv:hep-ph/9611232; PROSPINO2: http://www.thphys.uni-

heidelberg.de/~plehn/prospino/.
[21] M. L. Mangano *et al.*, J. High Energy Phys. 07 (2003) 001.
[22] S. Y. Choi, M. Drees, A. Freitas, and P. M. Zerwas, Phys. Rev. D **78**, 095007 (2008); J. Alwall, D. Rainwater, and T. Plehn, Phys. Rev. D **76**, 055006 (2007).
[23] Z. Chacko and E. Ponton, J. High Energy Phys. 11 (2003) 024.
[24] A. D. Medina and C. E. M. Wagner, J. High Energy Phys. 12 (2006) 037.
[25] D. E. Kaplan, G. D. Kribs, and M. Schmaltz, Phys. Rev. D **62**, 035010 (2000); Z. Chacko, M. A. Luty, A. E. Nelson, and E. Ponton, J. High Energy Phys. 01 (2000) 003.
[26] M. Schmaltz and W. Skiba, Phys. Rev. D **62**, 095004 (2000); **62**, 095005 (2000); H. Baer, A. Belyaev, T. Krupovnickas, and X. Tata, Phys. Rev. D **65**, 075024 (2002).